Boundary-Layer Meteorology

Surface energy fluxes during the total solar eclipse over Ny-Ålesund, Svalbard, on 20 March 2015

Alexander Schulz[1], Carsten Schaller[2], Marion Maturilli[1], Julia Boike[1], Christoph Ritter[1] and Thomas Foken[3*]

[1]Alfred Wegener Institute, Helmholtz Centre for Polar and Marine Research, Potsdam, Germany
[2]University of Münster, Institute of Landscape Ecology, Climatology Group, Münster, Germany
[3]University of Bayreuth, Bayreuth Center of Ecology and Environmental Research (BayCEER), Bayreuth, Germany

Abstract

On 20 March 2015, a total solar eclipse occurred over Ny-Ålesund (78.9° N, 11.9° E), Svalbard, under ideal conditions with clear sky. The cycle of the radiation fluxes is comparable with other experiments during eclipses, with even the upward longwave radiation showing significant changes, with a delay to the shortwave radiation and a slowly linear increase after the totality. Also, under polar conditions, an increase of the wind velocity before and a decrease after the totality was found, which is an indicator of the generation of an "Eclipse cyclone". This change of the wind direction generated a local wind system with a near-surface-layer katabatic flow. During the eclipse, a remarkably large sensible heat flux was observed. The turbulent fluxes were analysed using a wavelet technique with 1-minute time resolution, which is the ideal method for investigating these highly non-steady conditions. No influences on the boundary layer structure as measured with radiosondes were found, with the exception of a wind direction change during the eclipse cyclone below the shallow inversion layer.

Keywords: total solar eclipse, sensible heat flux, radiation, eclipse cyclone, Ny-Ålesund

1 Introduction

Solar eclipses are not only a special event for astronomers but also for meteorologists. Special meteorological campaigns during such events have been carried out for a long time (Anderson, 1999; Hinzpeter and Wörner, 1955). Most of these investigations made measurements of the short- and long-wave radiation components, but in the last 20 years measurements of the turbulent fluxes of sensible and latent heat or even trace gas fluxes have also been included in such measuring programs (Ahrens et al., 2001; Aplin and Harrison, 2003; Behrens et al., 2016; Eaton et al., 1997; Fabian et al., 2001; Foken et al., 2001; Founda et al., 2007; Mauder et al., 2007; Nymphas et al., 2012; Satyaningsih et al., 2016). Up to now, only one investigation of a total solar eclipse under conditions of high latitude, that of 23 November 2003 over Antarctica, has been published (Kameda et al., 2009). Such studies make it possible to investigate the interaction of radiation and turbulent fluxes and the relevant response times under the situation of a nearly abrupt change of the radiation fluxes. This is not possible during sun rise and sun set because of the slow change of the radiation. One other possibility is provided by abruptly changing cloudiness

at high altitudes, such as on the Tibetan Plateau, with a nearly aerosol-free atmosphere.

A solar eclipse is like a laboratory experiment for response times of the energy fluxes and the interaction of these fluxes. The observed phenomena of an "eclipse cyclone" (Clayton, 1901) also offers the opportunity to study how changes of the energy input can generate changes in the pressure field.

At one of the most northerly research stations, at Ny-Ålesund (78.9° N, 11.9° E) on the archipelago of Svalbard (Uttal et al., 2016), a total eclipse occurred on 20 March 2015, with the time of totality between 1009, 52 sec UTC and 1012, 11 sec UTC and a duration of the totality of 2 min 20 sec. The elevation of the sun above the horizon was about 10° at totality and about 11° at noon, and the land was fully covered with snow while the ocean was ice-free. The synoptic situation was optimal for studying the eclipse, with a cloud-free atmosphere under the influence of a high-pressure area over the Greenland Sea. Pressure was nearly constant (decrease of 3 hPa per 12 hours).

The Ny-Ålesund site is well equipped for such investigation due to the presence of a Baseline Surface Radiation Station (BSRN) since 1992 (Maturilli et al., 2015) and two flux measuring stations, one near the BSRN station (Jocher et al., 2012) and one about 1.8 km away on a wet and undisturbed permafrost area
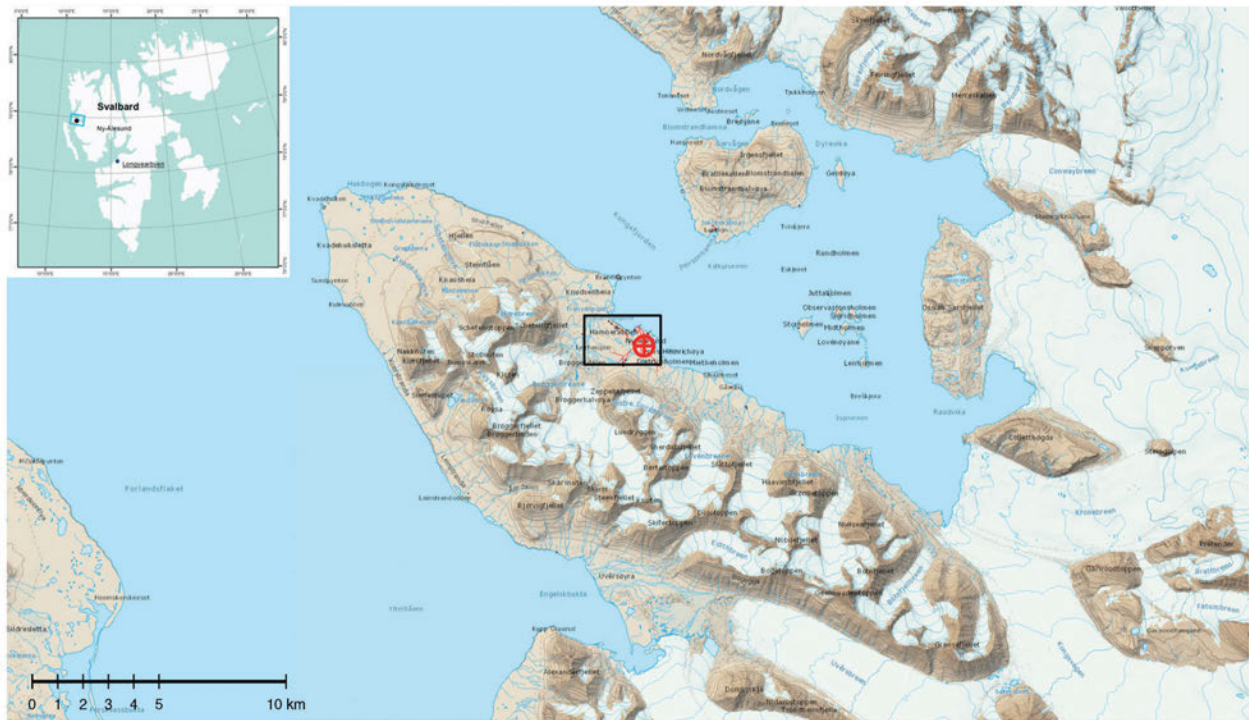
Figure 1: Location of Ny-Ålesund at the Kongsfjorden on Svalbard (map was obtained from the Norwegian Polar Institute: http://svalbardkartet.npolar.no/html5/index.html?viewer=svalbardkartet)

(Westermann et al., 2009), with both operating nearly continuously for about 5–10 years. The flux stations were equipped to measure net radiation. It was possible to investigate the radiation fluxes as well as the turbulent fluxes with a time resolution of one minute, to investigate response times with a high resolution in time. All of these measuring systems were operated by the Alfred Wegener Institute.

The special interest of solar eclipse measurements at high latitudes is the effect of a very high albedo. Therefore the absolute effect on the upward longwave radiation component and on the available energy at the surface should be low. This may reduce the effect on turbulent fluxes and possible circulation patterns that were found during eclipses in mid latitudes. Such investigations are important for weather and climate models, because in the frequently only weakly stable Arctic boundary layer, even small perturbations can have a strong impact on stability and boundary layer altitude.

The radiation data of the BSRN station during the total solar eclipse were already published by Maturilli and Ritter (2016a; 2016b).

2 Material and methods

2.1 The Ny-Ålesund site

Ny-Ålesund is located at the south-west side of the Kongsfjorden, with the Zeppelin Mountain to the south and the Bayelva valley and Brøggerbreen glacier in a west to south-westerly direction (Fig. 1). The common south-easterly near-surface atmospheric flow along the fjord axis (Beine et al., 2001; Maturilli et al., 2013) – coming from the Kongsvegen glacier – is, during periods with low wind speeds, interrupted by the katabatic flow from the glaciers located to the south, and under strong synoptic forcing, by flow from the ocean north-west of the site (Jocher et al., 2012).

The locations of the measurement sites used in this study are given in Fig. 2, with the BSRN station south of the observatory at Ny-Ålesund and the Ny-Ålesund eddy-covariance station a further 300 m to the southwest. The Bayelva eddy-covariance station is about 1.8 km westward of the other sites.

Polar day and polar night conditions are from 18 April to 24 August and from 24 October to 18 February, respectively. On 20 March, the diurnal cycle is characterized by regular day and night-time conditions, with the sun above the horizon for about 12 hours. The solar eclipse occurred at 1011 UTC, when the sun was above the mountains, allowing observations of the partial and total solar eclipse phases. About 15 minutes after the end of the eclipse, the BSRN station was in the shadow of the Zeppelin Mountain, while the eddy-covariance station Ny-Ålesund (NA-EC) was already in the shadow of the mountain about 30 minutes after totality and the Bayelva eddy-covariance station (BA-EC) was in shadow up to the totality.
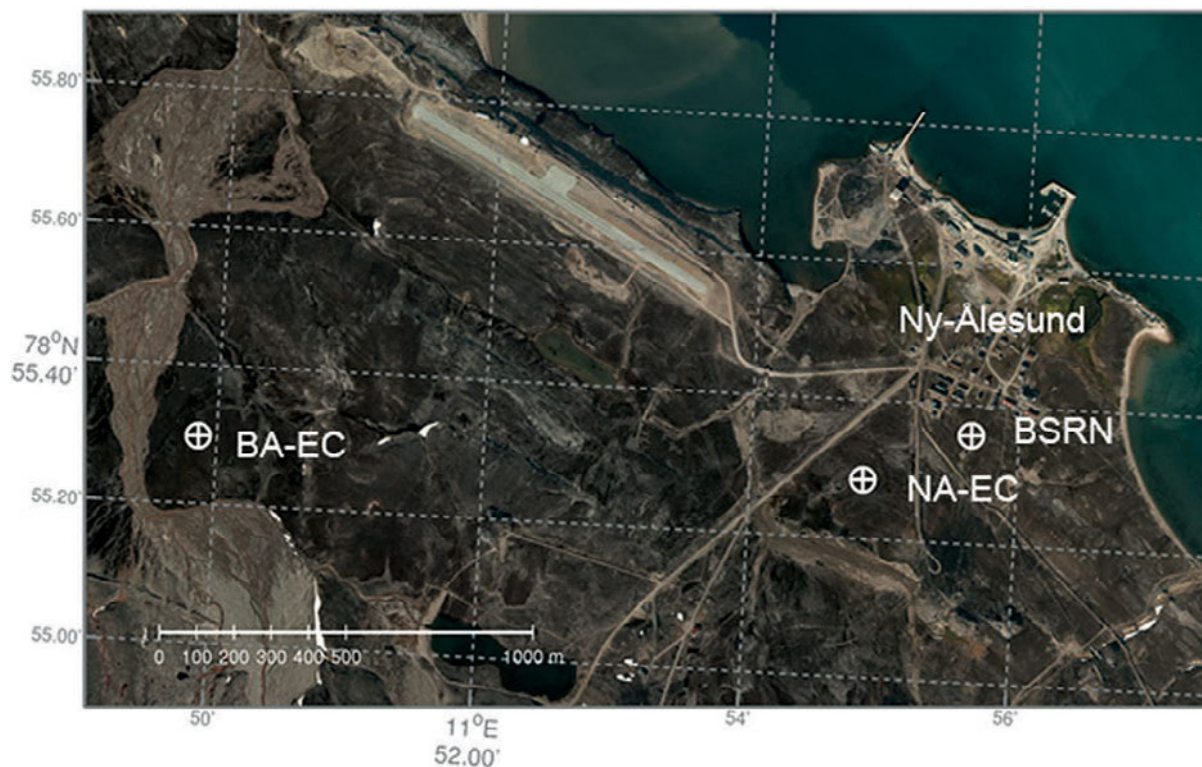
Figure 2: Location of the measuring sites at Ny-Ålesund: BSRN: Baseline Surface Radiation Station with radiation and synoptic measurements; NA-EC: Ny-Ålesund eddy-covariance site; BA-EC: Bayelva eddy-covariance site. (The aerial photograph was obtained from the Norwegian Polar Institute: http://svalbardkartet.npolar.no/html5/index.html?viewer=svalbardkartet)

2.2   Radiation measurements

The downward radiation components and the upward longwave radiation during the eclipse phase were measured at the BSRN site and, according to quality-control factors, independent measurements were made of direct and diffuse radiation in addition to the global radiation. The direct radiation was measured by a Kipp & Zonen CHP1 pyrheliometer on a Schulz & Partner solar tracker shared with the diffuse radiation measurement by a ball-shaded Kipp & Zonen CMP22. Global and reflected radiation was also detected by CMP22 instruments, while upward and downward longwave radiation components were obtained by Eppley PIR pyrgeometers (MATURILLI et al., 2015). The direct radiation was normalized to the horizontal plane. The ground beneath the radiation instrumentation setup was also snow-covered, with a snow layer of about 30 cm height as measured by a Jenoptik snow depth sensor. As low solar elevation angles limit the reliability of the albedo retrieval, the albedo value of 0.7 (error 6 %) was found for the end of the eclipse, with the highest solar elevation of nearly 11°. The longwave radiation measurements were temperature-corrected with three internal temperature sensors that confirmed the radiative cooling and indicated that the decrease in upward longwave radiation was not caused by changes in air temperature due to advection.

Radiation measurements at both eddy-covariance sites were made with a CNR4 Kipp and Zonen four component net radiometer (Ny-Ålesund EC site) and a NR01 Hukseflux four component net radiometer (Bayelva EC site).

The radiation measurements and all other meteorological parameters (temperature, wind etc.) were sampled with 2 s time interval.

2.3   Turbulence measurements

The turbulence measurements were made according to the recent recommendations for eddy-covariance measurements (AUBINET et al., 2012). Both sites were equipped with sonic anemometers CSAT3 (Campbell Sci. Inc.) and open path gas analysers 7500A (LI-COR Biosciences). Due to an additional mounted IRGASON (Campbell Sci. Inc.) we could minimize wind flow disturbance at the EC-NA system even for westerly winds, which occurred during totality. All necessary corrections and data quality tests (FOKEN et al., 2012) were applied in accordance with the software package TK3 (MAUDER and FOKEN, 2015a; 2015b), which is comparable with other available packages (FRATINI and MAUDER, 2014; MAUDER et al., 2008). The moisture-dependent corrections were not relevant due to the low air temperature (below $-15\,°C$) and the corresponding low absolute humidity. Therefore, the latent heat flux was always below the detection limit. The measuring heights were 2.1 m for the Ny-Ålesund EC site and 2.75 m for the Bayelva EC site.
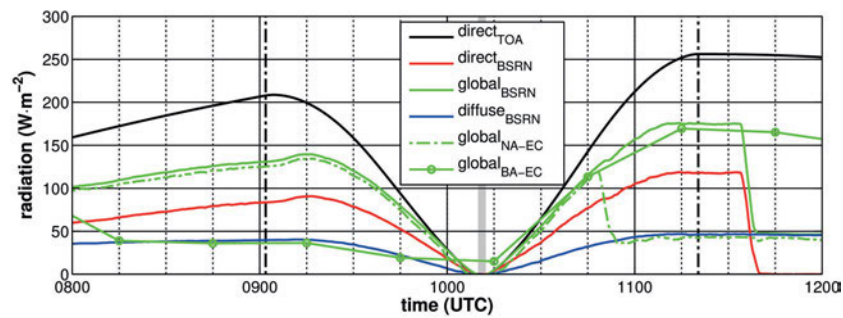
Figure 3: Cycle of the shortwave radiation during the solar eclipse at BSRN station. For comparison, the global radiation of Ny-Ålesund eddy-covariance site (NA-EC) and Bayelva eddy-covariance site (BA-EC) are given. The measurements are affected by the shadow of the Zeppelin Mountain up to the totality for BA-EC, beginning at 1050 for NA-EC, and beginning at 1135 for BSRN. For BA-EC only 30-minute averages are available, and all other data are from high resolution raw data. For comparison, in all figures the extra-terrestrial radiation (TOA: top of the atmosphere) is shown (the code was adapted from: AIR_SEA TOOLBOX (version 2.0: 8/9/99), Rich Pawlowicz) together with the begin of the partial eclipse (vertical dashed line), the period of totality (grey shadow), and the end of the partial eclipse (vertical dashed line).

A solar eclipse event is highly non-steady state. Under these conditions the eddy-covariance method fails all quality criteria (FOKEN AND WICHURA, 1996) and the calculated flux is questionable. The wavelet analysis offers a possibility for calculating the turbulent flux from the spectrum of the wavelet coefficients, even under these conditions (COLLINEAU AND BRUNET, 1993b; HANDORF AND FOKEN, 1997; KATUL AND PARLANGE, 1995; TREVIÑO AND ANDREAS, 1996). For steady state conditions, the wavelet and eddy-covariance methods are in very good agreement (SCHALLER et al., 2017). For the first time, this method was applied to calculate fluxes during a solar eclipse. This method offers the possibility of determining exact fluxes with a time resolution of about 1 minute, as with the radiation measurements. We applied the recently published calculation tool presented by SCHALLER et al. (2017) with a continuous wavelet transform with the Mexican hat wavelet, which provides an excellent resolution in the time domain. The flux can be calculated with the power spectra of the wavelet coefficient for a given time interval – in our case 1 minute. Thus it allows an exact localization of single events in time (COLLINEAU AND BRUNET, 1993a). For more details see the given reference.

2.4 Radiosonde measurements

Before the partial eclipse (0839 UTC), during the total eclipse (1010 UTC), and after (1114 UTC) the partial eclipse, three Vaisala RS92 radiosondes were launched from Ny-Ålesund with an ascent rate of 5 ms^{-1}. The Ny-Ålesund radiosonde programme is certified by the Global Climate Observing Systems (GCOS) Reference Upper-Air Network (GRUAN), providing radiosonde data in reference quality. The radiosonde launched at 1114 UTC has therefore been processed by GRUAN, and the data are available with quantitative uncertainty values for every measurement point (SOMMER et al., 2012). The air temperature profiles in the lowermost

300 m show a surface-based inversion below 100 m altitude and stable conditions in the atmospheric boundary layer. Within the typical error band, no air temperature changes during the eclipse could be detected. The profiles were presented by MATURILLI and RITTER (2016b). With acceptance of the large error, some results of the wind direction are shown in Section 3.2.

3 Results and discussion

3.1 Radiation and temperature

Because of the cloud-free clear sky and the low aerosol density, the short wave radiation components show an ideal cycle of a solar eclipse (Fig. 3). The aerosol optical depth at a wavelength of 500 nm had a maximum of 0.07 derived by photometer SP1A (Schulz & Partner, Buckow, Germany), which is lower than the monthly average for March at Ny-Ålesund (TOMASI et al., 2015). About two thirds of the global radiation is direct incoming solar radiation. The diffuse radiation at the beginning and the end is nearly the only contribution to the global radiation, when the site was in the shadow of the Zeppelin Mountain, which indicates the low aerosol concentration. Besides the lower quality classes of the sensors at the eddy-covariance sites, the global radiation is comparable with the BSRN station (Fig. 3) and can be used for the further discussion. The shortwave upward radiation follows the cycle of the downward radiation (not shown). The solar elevation was too low for an exact determination of the albedo (see Section 2.2).

The ratio of the longwave radiation components is an indicator for the clear sky (Fig. 4). The longwave upward radiation is, to a large extent, driven by surface temperature and follows – with a delay – the shortwave radiation. After the totality, the increase of the longwave upward radiation goes much slower, with a linear increase, than the increase of the shortwave radiation.
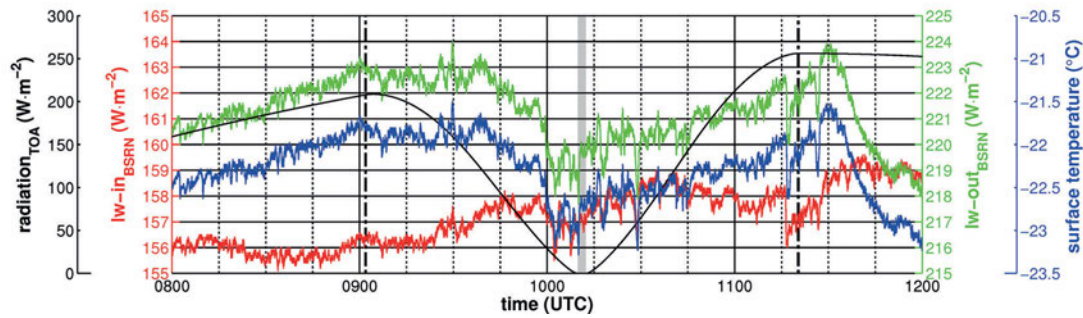
Figure 4: Cycle of the longwave downward radiation (lw-in), longwave upward radiation (lw-out), and the surface temperature during the solar eclipse at BSRN station.
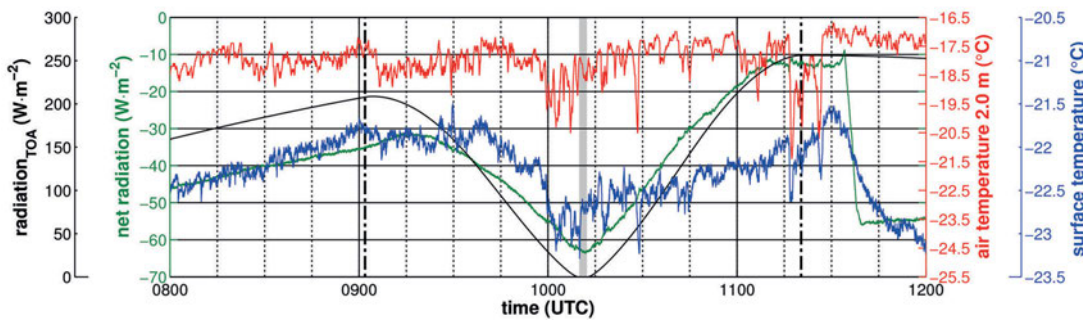

Figure 5: Air temperature and surface temperature and net radiation at BSRN station, which is, from 1135, in the shadow of the Zeppelin Mountain. The negative values of the net radiation indicate a loss of energy at the surface.

Table 1: Comparison of radiation measurements during the solar eclipse on 23 November 2003 in Antarctica (KAMEDA et al., 2009) and on 20 March 2015 at Svalbard

Parameter	Dome Fuji, Antarctica, 77° S 3810 m a.s.l.	Svalbard, 79° N 15 m a.s.l. (BSRN) 27 m a.s.l. (NA-EC)
	23 November 2003	20 March 2015
Global radiation before and after the partial eclipse	203 and 269 Wm^{-2}	131 and 175 Wm^{-2}
Air temperature before the partial eclipse and effect of the cooling	−51 °C, ca. 3 K	−18 °C, ca. 2 K
Net radiation before the partial eclipse and during the totality[*]	−5 Wm^{-2} and −50 Wm^{-2}	−35 Wm^{-2} and −63 Wm^{-2}
Albedo	0.85	about 0.7

[*] negative values: Loss of energy at the surface

This kind of hysteresis was also found during other total eclipses (FOKEN et al., 2001). The surface temperature was calculated with the Stefan-Boltzmann law for a grey body with emissivity of 0.985 from outgoing longwave radiation measurement and follows the longwave radiation exactly.

The air temperature at 2.0 m and the surface temperature follow, with a short delay, the shortwave and net radiation. The air temperature increase after the totality is much faster than the surface temperature and follows the increase of the radiation. The high air temperature fluctuations of the air temperature shortly before the totality are discussed in Section 3.2. A time shift of several minutes between the totality and the minimum in

air temperature (ANDERSON, 1999; EATON et al., 1997; FOKEN et al., 2001; FOUNDA et al., 2007) could not be found. The net radiation is strongly related to the incoming short wave radiation. Due to the higher upward than downward longwave radiation, there is a radiative energy flux of −63 Wm^{-2} from the surface to the atmosphere during the totality.

Table 1 compares the two experiments during a solar eclipse at high latitudes (KAMEDA et al., 2009, and this study). The eclipse in Antarctica was about one month before the solar maximum while the eclipse at Svalbard was exactly at the spring equinox. Both eclipses occurred shortly before noon. Therefore, the incoming shortwave radiation was about 100 Wm^{-2} higher in
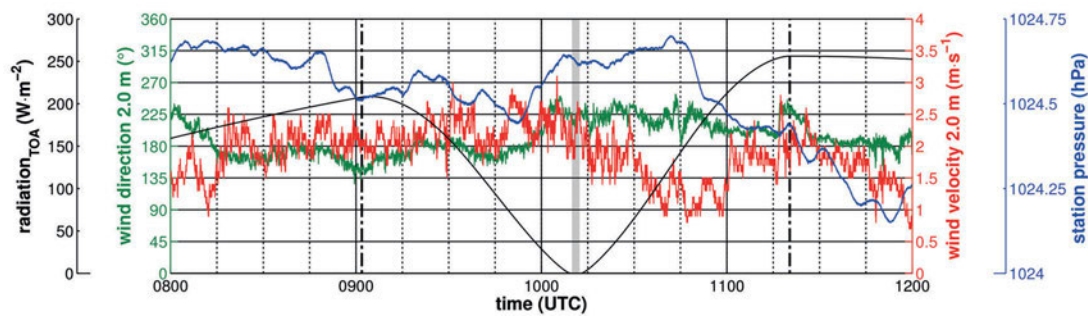
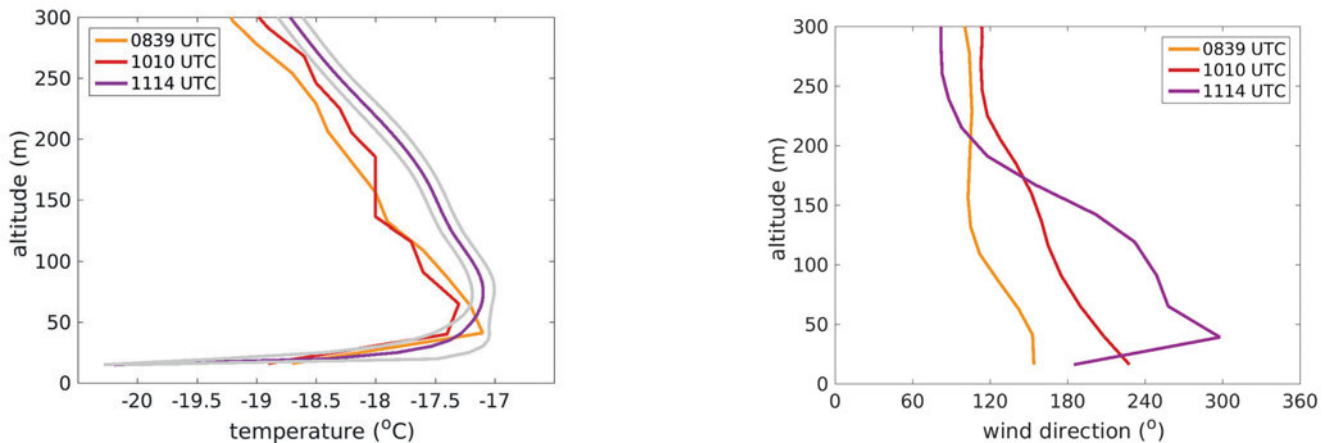**Figure 6:** Pressure, wind velocity and direction at BSRN station.

Figure 7: Radiosoundings of the air temperature (left) and the wind direction (right) before (0839) and after (1114) eclipse and during the totality (1010). Remark: The values below 150 m did not fulfil the strong GRUAN quality criteria. Left figure adapted from MATURILLI and RITTER (2016b) with kind permission of © Authors 2016, all rights reserved.

Antarctica, but the air temperature was much lower due to the location of the Dome Fuji station on the Antarctic Plateau (3810 m a.s.l.). Due to the low air temperature at this altitude in comparison to the air temperature at Ny-Ålesund, the difference between the up- and downward longwave radiation, and therefore the net radiation, was lower.

3.2 Wind velocity

From several solar eclipse experiments is reported (APLIN and HARRISON, 2003; FOKEN et al., 2001; NYMPHAS et al., 2012) that the wind velocity increases shortly before the totality and decreases with a minimum after the totality, with a remarkable change of the wind direction. The situation is comparable with the passage of a large cumulus or a cumulonimbus cloud and is known as an "Eclipse cyclone" (CLAYTON, 1901). Such an eclipse cyclone has a diameter of approximately 2000 km and a high pressure area allows its generation. This phenomenon was investigated for the 11 August 1999 eclipse over Europe by APLIN and HARRISON (2003) and PROVOD (2010). The situation at Ny-Ålesund is more complex due to the changes between the typical fjord-parallel wind and the westerly katabatic wind from the glacier (see Section 2.1), but the optimal anticyclonal conditions were present.

The wind velocity and direction are shown in Fig. 6. A katabatic wind from the south was present over the whole day, passing the Zeppelin Mountain. About 10 minutes before totality the wind velocity increased and the direction shifted about 45° westward, so that the katabatic wind then came from the Brøggerbreen glacier. About 10 minutes after the totality the wind velocity decreased and had a minimum about half an hour later. It is the typical picture seen during other eclipses (Table 2). The anticyclone over the Greenland Sea was the optimum background condition for its generation. The shift in the wind direction is probably larger due to orographic effects and relief-induced katabatic flows. The situation is in accordance with a pressure decrease before the totality and an increase after the totality of about 0.3 hPa.

While keeping in mind that the retrieval of wind direction from radiosondes while balloons are still in the first part of the ascent is subject to potentially large errors, we analysed the three soundings before and after the partial eclipse and within the totality; these are shown in Fig. 7. The change of the wind direction during the totality (Fig. 6) is only visible below the inversion layer (Fig. 7). After the eclipse, the wind direction at the ground turned again to the south (Fig. 6 and 7, near the ground), while below the inversion there was still a zone

Table 2: Effect of a solar eclipse on wind velocity and direction

eclipse and location	wind velocity before the partial eclipse, with reduction	shift in wind direction	reference
11 August 1999 Camborne, U.K.	$3.0\,\mathrm{ms^{-1}}$, ca. $-2.0\,\mathrm{ms^{-1}}$	140° to 130°	APLIN and HARRISON (2003)
11 August 1999 Freising, Germany	$2.5\,\mathrm{ms^{-1}}$, ca. $-1.5\,\mathrm{ms^{-1}}$		FOKEN et al. (2001)
11 August 1999 Fülöpháza, Hungary	$2.5\,\mathrm{ms^{-1}}$, ca. $-1.5\,\mathrm{ms^{-1}}$		FOKEN et al. (2001)
11 August 1999 Plittersdorf, Germany	$1.5\,\mathrm{ms^{-1}}$, ca. $-1.0\,\mathrm{ms^{-1}}$		AHRENS et al. (2001)
23 November 2003 Dome Fuji, Antarctica	$6.5\,\mathrm{ms^{-1}}$, ca. $-0.3\,\mathrm{ms^{-1}}$	< 5°	KAMEDA et al. (2009)
29 March 2006 Ibadan, Nigeria	$2.0\,\mathrm{ms^{-1}}$, ca. $-1.0\,\mathrm{ms^{-1}}$		NYMPHAS et al. (2012)
20 March 2015 Ny-Ålesund, Svalbard	$2.5\,\mathrm{ms^{-1}}$, ca. $-1.5\,\mathrm{ms^{-1}}$	180° to 225°	this study

of westerly wind (Fig. 7). Above the inversion, also visible in wind lidar measurements (not shown), no effect of the eclipse was found.

3.3 Turbulent fluxes

Turbulent fluxes were investigated during solar eclipses in the last 20 years (BEHRENS et al., 2016; EATON et al., 1997; FOKEN et al., 2001; KAMEDA et al., 2009; MAUDER et al., 2007; NYMPHAS et al., 2012) in addition to the classical radiation measurements. While a strong radiative forcing is usually closely correlated with the fluxes, with a time shift of only a few minutes, the situation under polar conditions is much more complicated. In the following, only some ideas are presented to explain the difficult situations. Only the sensible heat flux could be analysed, because the latent was – due to the low water vapour concentration – below the detection limit.

The change of the wind field was more pronounced in the friction velocity than in the wind velocity. The friction velocity increased significantly at the beginning of the totality (Fig. 8a) and again shortly before the end of the partial eclipse, when the wind field returned to the situation before the partial eclipse. This effect was only seen at EC-NA and not at EC-BA, which was in the shadow of the Zeppelin Mountain during the whole eclipse.

During the eclipse, the net radiation flux was from the surface to the atmosphere (negative values in Fig. 5; usually the micrometeorological definition would be a positive flux) with a cooling at the surface. The sensible heat flux compensates for this energy loss and is downward orientated. In Fig. 8b it is shown with a negative sign according to the micrometeorological definition. The 5-minute averages, which have a low data quality due to the non-steady state conditions, nearly compensate for the net radiation. The wavelet fluxes with a high

time resolution of 1 minute are much larger, but they correspond very well to the dynamical effect due to the increase of the friction velocity for a short time-period. Additional effects of advection cannot be excluded. But most of the time, the sensible heat flux was nearly zero, within the detection limit (MAUDER et al., 2006).

The air temperature profile indicates the same direction of the sensible heat flux (Fig. 9). Additionally, the surface temperature was calculated with the Stefan-Boltzmann law for a grey body with emissivity of 0.985 from outgoing longwave radiation measurement (Kipp & Zonen CNR4). The near-surface layer is well mixed until shortly after the totality, because identical air temperature differences between 0.5 m and 1 m, as well as between 1 m und 2 m, are a criterion for the classical log-lin-temperature profile. With decreasing wind velocity and also friction velocity, the lower layer of 0.5 m and below no longer follows the upper layer (> 1 m), which is a criterion for a decoupling near the surface. Such decoupling situations between the surface and the air layers a few decimeters above the surface were well investigated for Ny-Ålesund (LÜERS and BAREISS, 2010) and also known for Antarctica (SODEMANN and FOKEN, 2005). A cooling started when the EC-NA station was in the shadow of the Zeppelin Mountain at 1050. Together with the increasing wind velocity, the air temperature dropped nearly 3 degrees, probably due to a stronger katabatic flow. This situation is combined with a strong positive sensible heat flux, which can only be explained by advection of warm air after the situation of decoupling. Furthermore, after the eclipse at 1140 such a situation was again observed. A similarly atypical situation was also found by KAMEDA et al. (2009) for the solar eclipse in Antarctica using a simple bulk approach.

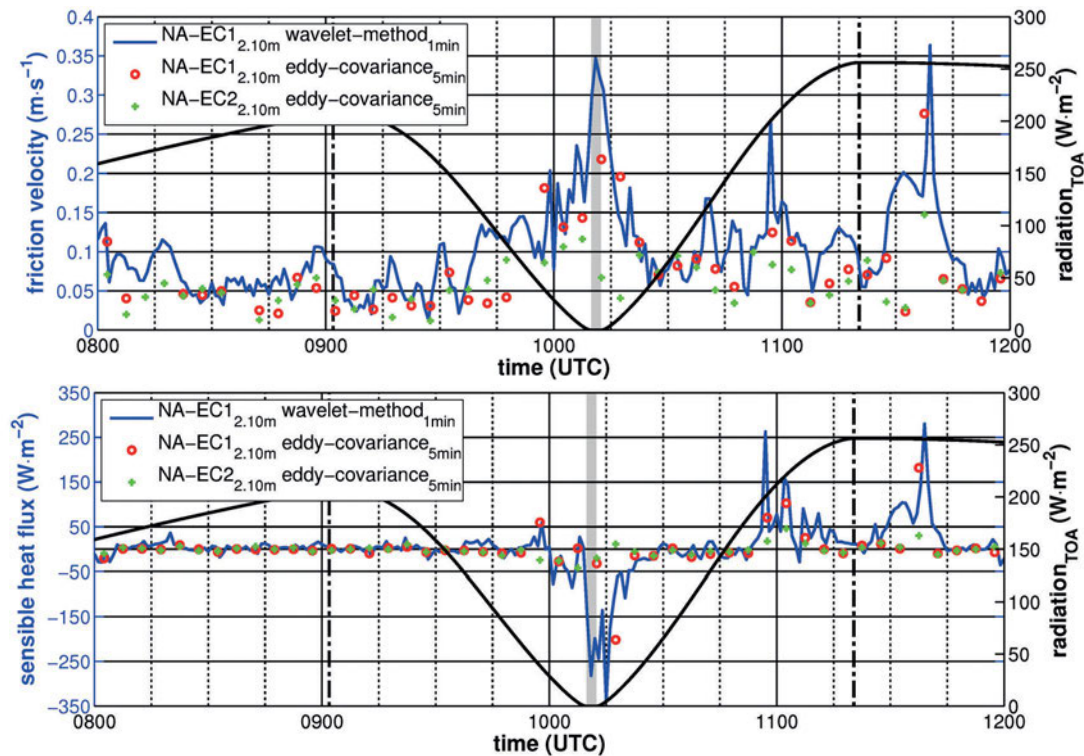Because the Bayelva site was in the shadow of the Zeppelin Mountain up to the totality and was further-

Figure 8: Friction velocity (above) and sensible heat flux (below) measured at Ny-Ålesund EC site, measured with wavelet technique and eddy-covariance technique (5-minute average). For visualization of possible flow distortion effects during the eclipse, the second turbulence measuring complex was included in this figure (EC-NA1: CSAT3 and LiCor 7500A; EC-NA2: IRGASON).
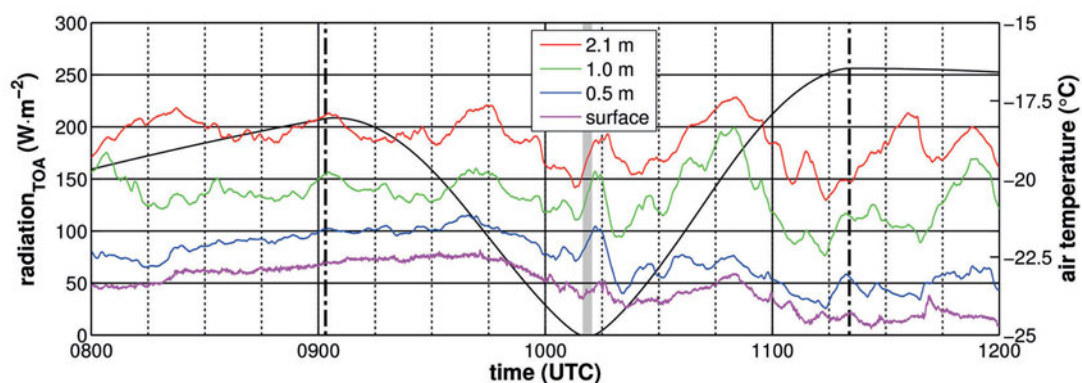

Figure 9: Air temperature profile and surface temperature near the Ny-Ålesund EC site.

more in a wind shadow, no significant sensible heat fluxes could be detected.

4 Conclusions

The opportunity to investigate turbulent and radiative fluxes during a total solar eclipse in polar regions on 20 March 2015 at Ny-Ålesund, Svalbard, was ideal due to a cloud-free, clear sky. This was the second time that turbulent fluxes were measured under these conditions. The research site was highly equipped with meteorological instrumentation, so that a combined radiation and turbulence experiment could be realized. Despite the high albedo of 0.7 over the snow-covered surface, all radiation fluxes provided a picture comparable with other

eclipses. Even the change in the upward longwave radiation was similar, with a time lag between the beginning of the partial eclipse and the decrease of the radiation and a slow, nearly linear, increase after the totality.

The increase of the wind velocity before the totality and the decrease after the totality – compared with a pressure decrease and increase before and after the totality, respectively – was a clear indication of the eclipse cyclone. This is quite interesting because of the low radiation forcing (in comparison with mid-latitude eclipses) and the strong forcing by the air temperature difference between the open ocean and the snow and ice covered land (compare with Fig. 1). Due to the orography, the change in the wind direction of 45° was much larger than for other experiments, with the generation of a katabatic

flow and significant influences on air temperature and turbulent fluxes, which did not follow typical conditions during eclipses.

During the totality, the averaged sensible heat flux nearly compensated for the energy loss at the surface due to longwave cooling, but due to a dynamic effect one-minute sensible heat fluxes were much larger, which was probably connected to advection. In general, the turbulent fluxes showed a very complex picture, with well-mixed situations and periods with decoupling of the layer nearest to the surface and higher layers. Such decoupling situations must be taken into account in the cases of stable stratification, low wind conditions and low radiation forcing. Even small changes of the wind flow are related to significant changes in the energy fluxes and this makes the study – and also the modelling – of polar meteorological situations so complex and sensitive. The measurements obtained during the solar eclipses underline this statement. The successful application of the wavelet method for calculation of turbulent fluxes offers the possibility of also applying this tool for other situations with non-steady state fluxes, which are typical under polar conditions.

5 Acknowledgement

References

Ahrens, D., M.G. Iziomon, L. Jaeger, A. Matzarakis, H. Mayer, 2001: Impacts of the solar eclipse of 11 August 1999 on routinely recorded meteorological and air quality data in south-west Germany. – Meteorol. Z. **10**, 215–223. DOI:10.1127/0941-2948/2001/0010-0215.

Anderson, J., 1999. Meteorological changes during a solar eclipse. – Weather **54**, 207–251. DOI:10.1002/j.1477-8696.1999.tb06465.x.

Aplin, K.L., R.G. Harrison, 2003: Meteorological effects of the eclipse of 11 August 1999 in cloudy and clear conditions. – Proceedings of the Royal Society of London A: Mathematical, Physical and Engineering Sciences **459**, 353–371. DOI:10.1098/rspa.2002.1042.

Aubinet, M., T. Vesala, D. Papale (Eds), 2012: Eddy Covariance: A Practical Guide to Measurement and Data Analysis. – Springer, Dordrecht, Heidelberg, London, New York, 438 pp. DOI:10.1007/978-94-007-2351-1.

Behrens, K., F. Beyrich, R. Becker, L. Doppler, U. Rummel, 2016: Strahlungs- und Energieflüsse während der partiellen Sonnenfinsternis am 20.3.2015 in Lindenberg. – Mitteilungen DMG 2/2016, 9–10.

Beine, J.H., S. Argentini, A. Maurizi, G. Mastrantonio, A. Viola, 2001: The local wind field at Ny-Ålesund and the Zeppelin mountain at Svalbard. Meteorol. – Atmos. Phys. **78**, 107–113. DOI:10.1007/s007030170009.

Clayton, H.H., 1901. The eclipse cyclone and the diurnal cyclones. – Annals of the Astronomical Observatory of Harvard College **41**, 5–35.

Collineau, S., Y. Brunet, 1993a: Detection of turbulent coherent motions in a forest canopy. Part I: Wavelet analysis. – Bound.-Layer Meteor. **65**, 357–379. DOI:10.1007/BF00707033.

Collineau, S., Y. Brunet, 1993b: Detection of turbulent coherent motions in a forest canopy. Part II: Time-scales and conditional averages. – Bound.-Layer Meteor. **66**, 49–73. DOI:10.1007/BF00705459.

Eaton, F.D., J.R. Hines, W.H. Hatch, R.M. Cionco, J. Byers, D. Garvey, D.R. Miller, 1997: Solar eclipse effects in the planetary boundary layer over a desert. – Bound.-Layer Meteor. **83**, 331–346. DOI:10.1023/A:1000219210055.

Fabian, P., M. Winterhalter, B. Rappenglück, H. Reitmayer, A. Stohl, H. Schlager, T. Foken, B. Wichura, H. Berresheim, K.-H. Häberle, T. Kartschall, 2001: The BaySoFi campaign – Measurements carried out during the total solar eclipse of August 11, 1999. –Meteorol. Z. **10**, 165–170. DOI:10.1127/0941-2948/2001/0010-0165.

Foken, T., B. Wichura, 1996: Tools for quality assessment of surface-based flux measurements. – Agrical. Forest Meteor. **78**, 83–105. DOI:10.1016/0168-1923(95)02248-1.

Foken, T., B. Wichura, O. Klemm, J. Gerchau, M. Winterhalter, T. Weidinger, 2001: Micrometeorological conditions during the total solar eclipse of August 11,1999. – Meteorol. Z. **10**, 171–178. DOI:10.1127/0941-2948/2001/0010-0171.

Foken, T., R. Leuning, S.P. Oncley, M. Mauder, M. Aubinet, 2012: Corrections and data quality. – In: M. Aubinet, T. Vesala, D. Papale (Eds): Eddy Covariance: A Practical Guide to Measurement and Data Analysis. – Springer, Dordrecht, Heidelberg, London, New York, 85–131. DOI:10.1007/978-94-007-2351-1_4.

Founda, D., D. Melas, S. Lykoudis, I. Lisaridis, E. Gerasopolous, G. Kouvarakis, M. Petrakis, C. Zerefos, 2007: The effect of the total solar eclipse of 29 March 2006 on meteorological variables in Greece. – Atmos. Chem. Phys. **7**, 5543–5553. DOI:10.5194/acp-7-5543-2007.

Fratini, G., M. Mauder, 2014: Towards a consistent eddy-covariance processing: an intercomparison of EddyPro and TK3. – Atmos. Meas. Techn. **7**, 2273–2281. DOI:10.5194/amt-7-2273-2014.

Handorf, D., T. Foken, 1997: Analysis of turbulent structure over an Antarctic ice shelf by means of wavelet transformation, 12th Symosion on Boundary Layer and Turbulence. – Amer. Meteor. Soc., Vancouver BC, Canada, 245–246.

Hinzpeter, H., H. Wörner, 1955. Die Strahlungsmessungen in Potsdam und Persnäs. – In: Skeib, G. (Ed.): Die Sonnenfinsternis am 30. Juni 1954. – Veröff. Meteorol. & Hydrol. Dienstes DDR, 5–23.

Jocher, G., F. Karner, C. Ritter, R. Neuber, K. Dethloff, F. Obleitner, J. Reuder, T. Foken, 2012: The Near-Surface Small-Scale Spatial and Temporal Variability of Sensible and Latent Heat Exchange in the Svalbard Region: A Case Study. – ISRN Meteor. **2012**, 357925. DOI:10.5402/2012/357925.

Kameda, T., K. Fujita, O. Sugita, N. Hirasawa, 2009: Total solar eclipse over Antarctica on 23 November 2003 and its effects on the atmosphere and snow near the ice sheet surface at Dome Fuji. – J. Geophys. Res. **114**, D18115. DOI:10.1029/2009JD011886.

Katul, G.G., M.B. Parlange, 1995: Analysis of Land Surface Heat Fluxes Using the Orthonormal Wavelet Approach. – Water Res. Res. **31**, 2743–2749. DOI:10.1029/95WR00003.

Lüers, J., J. Bareiss, 2010: The effect of misleading surface temperature estimations on the sensible heat fluxes at a high Arctic site – the Arctic Turbulence Experiment 2006 on Svalbard (ARCTEX-2006). – Atmos. Chem. Phys. **10**, 157–168. DOI:10.5194/acp-10-157-2010.

MATURILLI, M., C. RITTER, 2016a: Basic and other measurements of radiation at station Ny-Ålesund (2015-03). – https://DOI.pangaea.de/10.1594/PANGAEA.854326.

MATURILLI, M., C. RITTER, 2016b: Surface radiation during the total solar eclipse over Ny-Ålesund, Svalbard, on 20 March 2015. – Earth Syst. Sci. Data **8**, 159–164. DOI:10.5194/essd-8-159-2016.

MATURILLI, M., A. HERBER, G. KÖNIG-LANGLO, 2013: Climatology and time series of surface meteorology in Ny-Ålesund, Svalbard. – Earth Syst. Sci. Data **5**, 155–163. DOI:10.5194/essd-5-155-2013.

MATURILLI, M., A. HERBER, G. KÖNIG-LANGLO, 2015. Surface radiation climatology for Ny-Ålesund, Svalbard (78.9° N), basic observations for trend detection. – Theor. Appl. Climat. **120**, 331–339. DOI:10.1007/s00704-014-1173-4.

MAUDER, M., T. FOKEN, 2015a: Eddy-Covariance software TK3. – Zenodo, published online, https://zenodo.org/record/20349.

MAUDER, M., T. FOKEN, 2015b: Documentation and Instruction Manual of the Eddy-Covariance. –Software Package TK3 (update). Arbeitsergebn., Univ. Bayreuth, Abt. Mikrometeorol. **62**, published online, https://zenodo.org/record/20349/files/ARBERG062.pdf.

MAUDER, M., C. LIEBETHAL, M. GÖCKEDE, J.-P. LEPS, F. BEYRICH, T. FOKEN, 2006: Processing and quality control of flux data during LITFASS-2003. – Bound.-Layer Meteor. **121**, 67–88. DOI:10.1007/s10546-006-9094-0.

MAUDER, M., R.L. DESJARDINS, S.P. ONCLEY, J.I. MACPHERSON, 2007: Atmospheric response to a solar eclipse over a cotton field in Central California. – J. Appl. Meteorol. Climatol. **46**, 1792–1803. DOI:10.1175/2007JAMC1495.1.

MAUDER, M., T. FOKEN, R. CLEMENT, J. ELBERS, W. EUGSTER, T. GRÜNWALD, B. HEUSINKVELD, O. KOLLE, 2008: Quality control of CarboEurope flux data – Part 2: Inter-comparison of eddy-covariance software. – Biogeosci. **5**, 451–462. DOI:10.5194/bg-5-451-2008.

NYMPHAS, E.F., T.A. OTUNLA, M.O. ADENIYI, E.O. OLADIRAN, 2012: Impact of the total solar eclipse of 29 March 2006 on the surface energy fluxes at Ibadan, Nigeria. – J. Atmos. Solar-Terrest. Phys. **80**, 28–36. DOI:10.1016/j.jastp.2012.02.024.

PROVOD, M., 2010: Solar eclipse-induced lower atmosphere changes. – MSc Thesis, The University of Reading, Reading, 114 pp.

SATYANINGSIH, R., E. HERIYANTO, KADARSAH, T.A. NURAINI, J. RIZAL, A. SOPAHELUWAKAN, E. ALDRIAN, 2016: Impacts of the total solar eclipse of 9 March 2016 on meteorological parameters in Ternate. – J. Phys. Conf. Ser. **771**, 012014.

SCHALLER, C., M. GÖCKEDE, T. FOKEN, 2017: Flux calculation of short turbulent events – comparison of three methods. – Atmos. Meas. Techn. **10**, 869–880. DOI:10.5194/amt-10-869-2017.

SODEMANN, H., T. FOKEN, 2005: Special characteristics of the temperature structure near the surface. – Theor. Appl. Climate **80**, 81–89. DOI:10.1007/s00704-004-0092-1.

SOMMER, M., R. DIRKSEN, F. IMMLER, 2012: RS92 GRUAN Data Product Version 2 (RS92-GDP.2). – GRUAN Lead Centre, Offenbach. DOI:10.5676/GRUAN/RS92-GDP.2.

TOMASI, C., A.A. KOKHANOVSKY, A. LUPI, C. RITTER, A. SMIRNOV, N.T. O'NEILL, R.S. STONE, B.N. HOLBEN, S. NYEKI, C. WEHRLI, A. STOHL, M. MAZZOLA, C. LANCONELLI, V. VITALE, K. STEBEL, V. AALTONEN, G. DE LEEUW, E. RODRIGUEZ, A.B. HERBER, V.F. RADIONOV, T. ZIELINSKI, T. PETELSKI, S.M. SAKERIN, D.M. KABANOV, Y. XUE, L. MEI, L. ISTOMINA, R. WAGENER, B. MCARTHUR, P.S. SOBOLEWSKI, R. KIVI, Y. COURCOUX, P. LAROUCHE, S. BROCCARDO, S.J. PIKETH, 2015: Aerosol remote sensing in polar regions. – Earth-Sci. Rev. **140**, 108–157. DOI:10.1016/j.earscirev.2014.11.001.

TREVIÑO, G., E.L. ANDREAS, 1996: On wavelet analysis of nonstationary turbulence. – Bound.-Layer Meteor. **81**, 271–288. DOI:10.1007/BF02430332.

UTTAL, T., S. STARKWEATHER, J.R. DRUMMOND, T. VIHMA, A.P. MAKSHTAS, L.S. DARBY, J.F. BURKHART, C.J. COX, L.N. SCHMEISSER, T. HAIDEN, M. MATURILLI, M.D. SHUPE, G. DE BOER, A. SAHA, A.A. GRACHEV, S.M. CREPINSEK, L. BRUHWILER, B. GOODISON, B. MCARTHUR, V.P. WALDEN, E.J. DLUGOKENCKY, P.O.G. PERSSON, G. LESINS, T. LAURILA, J.A. OGREN, R. STONE, C.N. LONG, S. SHARMA, A. MASSLING, D.D. TURNER, D.M. STANITSKI, E. ASMI, M. AURELA, H. SKOV, K. ELEFTHERIADIS, A. VIRKKULA, A. PLATT, E.J. FØRLAND, Y. IIJIMA, I.E. NIELSEN, M.H. BERGIN, L. CANDLISH, N.S. ZIMOV, S.A. ZIMOV, N.T. O'NEILL, P.F. FOGAL, R. KIVI, E.A. KONOPLEVA-AKISH, J. VERLINDE, V.Y. KUSTOV, B. VASEL, V.M. IVAKHOV, Y. VIISANEN, J.M. INTRIERI, 2016: International Arctic Systems for Observing the Atmosphere: An International Polar Year Legacy Consortium. – Bull. Amer. Meteor. Soc. **97**, 1033–1056. DOI:10.1175/BAMS-D-14-00145.1.

WESTERMANN, S., J. LÜERS, M. LANGER, K. PIEL, J. BOIKE, 2009: The annual surface energy budget of a high-arctic permafrost site on Svalbard, Norway. – The Cryosph. **3**, 245–263. DOI:10.5194/tc-3-245-2009.